

Article

Strain Rate-Dependent Mechanical Response of Hydrate-Bearing Sediments under Plane Strain Condition

Qi Wu ¹, Yingjie Zhao ¹, Norimasa Yoshimoto ², Jinan Guan ^{3,*}, Yukio Nakata ², Shintaro Kajiyama ² and Masayuki Hyodo ²

¹ National Center for International Research on Deep Earth Drilling and Resource Development, Faculty of Engineering, China University of Geosciences, Wuhan 430074, China; giecwuqi@foxmail.com (Q.W.); yingjiezhao@cug.edu.cn (Y.Z.)

² Graduate School of Science and Technology for Innovation, Yamaguchi University, Yamaguchi 755-0097, Japan; nyoshi@yamaguchi-u.ac.jp (N.Y.); nakata@yamaguchi-u.ac.jp (Y.N.); skajiyama@yamanashi.ac.jp (S.K.); hyodo@yamaguchi-u.ac.jp (M.H.)

³ CAS Key Laboratory of Gas Hydrate, Guangdong Provincial Key Laboratory of New and Renewable Energy Research and Development, Guangzhou Institute of Energy Conversion, Guangzhou 510640, China

* Correspondence: guanja@ms.giec.ac.cn

Abstract: Natural gas hydrate has gained significant attention in recent years. To safely and sustainably exploit the natural gas from gas hydrate-bearing sediments, it is crucial to understand the long-term mechanical characteristics of the hydrate reservoir. In this study, the influence of hydrate and fine particles on the strain rate dependence of hydrate-bearing sediments under plane strain conditions has been studied. The experimental results show that the strain rate dependency of the mechanical properties of hydrate-bearing sediments is positively correlated with hydrate saturation instead of the morphology of hydrate in sediments. The residual strength of hydrate-bearing sediments is primarily controlled by the hydrate saturation and is independent of the strain rate. Changes in hydrate saturation and fines content can affect the relationship between the strain rate and shear band angle. Finally, the local volumetric expansion effect of hydrate-bearing sediments without fines content is more significant and shows a strong strain rate dependence characteristic. Overall, this study provides valuable insights into the long-term mechanical characteristics of hydrate reservoirs. These insights can contribute to the development of a constitutive model of hydrate-bearing sediments with time dependence in the future, which is meaningful to the exploitation of natural gas hydrate.

Keywords: methane hydrate; strain rate-dependent; fine particles; hydrate saturation; particle tracking velocimetry



Citation: Wu, Q.; Zhao, Y.; Yoshimoto, N.; Guan, J.; Nakata, Y.; Kajiyama, S.; Hyodo, M. Strain Rate-Dependent Mechanical Response of Hydrate-Bearing Sediments under Plane Strain Condition. *J. Mar. Sci. Eng.* **2023**, *11*, 1161. <https://doi.org/10.3390/jmse11061161>

Academic Editor: Dimitris Sakellariou

Received: 25 April 2023

Revised: 29 May 2023

Accepted: 30 May 2023

Published: 1 June 2023



Copyright: © 2023 by the authors. Licensee MDPI, Basel, Switzerland. This article is an open access article distributed under the terms and conditions of the Creative Commons Attribution (CC BY) license (<https://creativecommons.org/licenses/by/4.0/>).

1. Introduction

Natural gas hydrate (NGH) is an ice-like crystal formed from gas (mainly methane) and water in certain low-temperature and high-pressure conditions. It has garnered significant attention as a promising energy resource due to the sizable deposits discovered in marine sediments and permafrost regions across the globe. Different exploitation methods, such as the depressurization method [1,2], thermal stimulation method [3], chemical inhibitor injection method [4], and gas exchange method [5], etc., have been proposed for gas production from the NGH reservoir. In recent years, China and Japan have conducted short-term trial exploitation activities of marine hydrates, confirming the feasibility of NGH exploitation [6,7]. In the near future, more exploitation activities will be implemented with the aim of discovering and preventing engineering and geological issues that may arise from long-term NGH exploitation. In fact, the risks associated with NGH exploitation have been extensively discussed, such as wellbore instability and submarine landslides caused by hydrate decomposition, reservoir subsidence, and accompanying environmental

issues [8–10]. Facing the long-term demand for safe NGH exploitation, accurate prediction of reservoir mechanical response behavior is particularly important. In particular, the study of the time-dependent mechanical properties of hydrate-bearing sediment is fundamental and crucial for accurately predicting the mechanical response behavior of reservoirs over the long term.

The strength and stiffness of the sediments increased significantly with the increase in hydrate saturation by comparing the tri-axial shear test results of Toyoura sands with and without hydrate [11]. The volumetric strain of the hydrate-bearing sediments changed from compression to expansion with the increase in hydrate saturation in the plane strain shear test [12]. The magnitude of the hydrate contribution to the strength of the sediments depends on the hydrate saturation and cementation characteristics, as has been found by the acoustic wave measurement method [13,14]. Different hydrate occurrence patterns (pore-filling, grain-coating, cementing, and supporting) in the sediments also have been clearly observed with the micro-CT technique [15]. The hydrate formation in sediments containing fine particles was inherently displacive and segregated [16].

Various experimental conditions, such as confining pressure [17], temperature [18], hydrate occurrence habits [19], hydrate dissociation [20,21], and fine particle content [16,22], can affect the mechanical properties of hydrate-bearing sediments. Higher effective confining pressure increases the strength and stiffness of such sediments, while lower temperatures, which are more thermodynamically stable for hydrates, also increase their strength. The presence of fine particles in hydrate-bearing sediments leads to larger peak shear strength and more pronounced volumetric expansion behavior [23]. Additionally, studies have also investigated the effects of hydrate decomposition on the mechanical properties of hydrate-bearing sediments [24], revealing that the decomposition of hydrates significantly reduces their strength.

Some constitutive models describing the stress–strain relationship of hydrate-bearing sediments have also been proposed. Numerous researchers have modified traditional soil mechanics constitutive models to enable them to accurately describe the stress–strain characteristics of hydrate-bearing sediments, such as the Mohr–Coulomb model [25,26], Duncan–Chang model [19,27], and Critical State model [28,29]. Due to the ambiguous physical interpretation of certain parameters and the inability of most models to account for local changes in the internal structure of specimens, accurately reflecting the true stress–strain behaviors of hydrate-bearing sediments under specific conditions can be challenging. Especially, the existing constitutive models for hydrate-bearing sediments exhibit significant discrepancies among different researchers in predicting the mechanical response of reservoirs during long-term hydrate exploitation [30].

In summary, the factors that affect the mechanical properties of hydrate-bearing sediments have been qualitatively or semi-quantitatively studied; however, studies on the time-dependent mechanical properties of hydrate-bearing sediments are rare, even though they are particularly important for accurately predicting the mechanical response behavior of NGH reservoirs over the long term. Accurate prediction of the mechanical behavior of NGH reservoirs during the exploitation process is crucial to ensuring safety of NGH exploitation. The time-dependence of mechanical properties of hydrate-bearing sediment is mainly reflected in the strain rate dependence and creep characteristics [31,32], and strain rate dependence experiments are considered an efficient method to study the time-dependence of its mechanical properties. Considering the variability of hydrate reservoirs [33] and some geological phenomena, such as landslide, more like plane strain, it is also necessary to study the effect of hydrate and fine particles on the strain rate dependence under plane strain conditions.

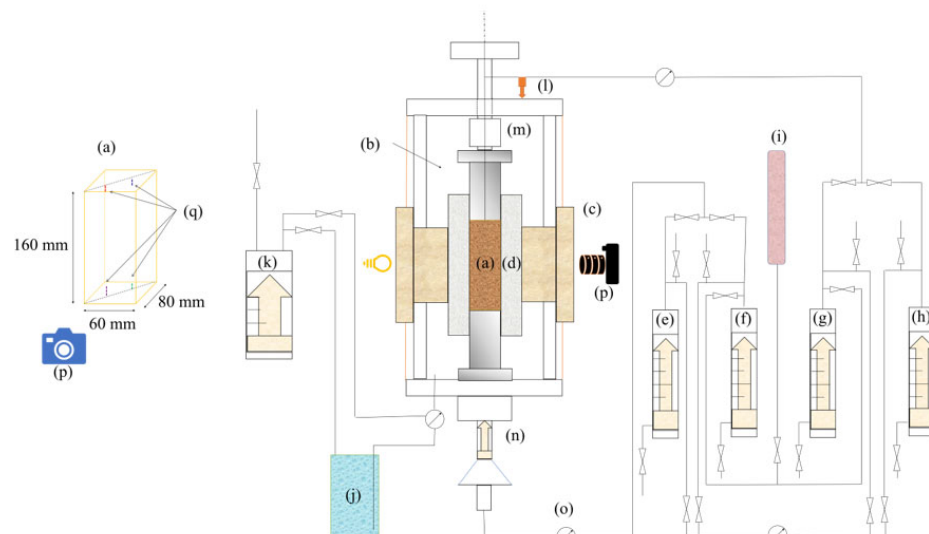
In this study, temperature-control and high-pressure plane strain shear test apparatuses with observation windows have been developed, and the influence of hydrate and fine particles on the strain rate dependence of hydrate-bearing sediments under plane strain conditions has been studied. The results are meaningful to develop the constitutive

model of hydrate-bearing sediments with time dependence in the future, and then achieve long-term accurate prediction of the mechanical characteristics of the hydrate reservoir.

2. Experimental Instruments and Procedure

2.1. Plane Strain Shear Test Apparatuses

Temperature-controlled and high-pressure plane strain shear test instruments with an observation window have been used to study the influence of hydrate and fine particles on the strain rate dependence of hydrate-bearing sediments. The schematic diagram of the instrument is shown in Figure 1. The size of the specimen is 60 mm (length) \times 80 mm (width) \times 160 mm (height). The pore and confining pressure of the specimen are controlled by different syringe pumps with an accuracy of ± 0.1 MPa. The maximum axial loading force that the instrument can provide is 200 kN, with a measurement accuracy of 0.2 kN. A latex film with a grid (the minimum unit is 2.5 mm \times 2.5 mm) attached to one side of the specimen can be used to measure the local deformation of the specimen. The picture of the specimen during the shearing process can be recorded by the electronic camera through the window on the instrument. More detailed information on these instruments can also be found in our previous reports [34]. Toyoura and the sand named Tb were used as the host sand in this study due to their similar particle size distributions to those found in the Nankai Trough NGH reservoirs [11]. The size distribution of these samples is shown in Figure 2, and Tb has a higher content of fine particles than Toyoura.



(a) Specimen; (b) pressure cell; (c) observation window; (d) confining plate; (e) lower syringe pump for water; (f) lower syringe pump for gas; (g) upper syringe pump for gas; (h) upper syringe pump for water; (i) methane gas cylinder; (j) cell liquid tank; (k) confining pressure amplifier; (l) displacement transducer; (m) load cell; (n) loading equipment; (o) pressure gauge; (p) camera; (q) thermocouple

Figure 1. The schematic diagram of high-pressure low-temperature plane strain testing apparatus.

2.2. Experimental Procedure

The experimental procedure can be divided into six steps: (1) Host sand preparation: wet host sand with a certain moisture content was filled into the mold in about 12 layers, and filter paper covered the upper and lower parts of the specimen. After that, the air inside the specimen was expelled by a vacuum pump and maintained the confining pressure at 0.2 MPa at the same time. (2) Hydrate generation: increased the pore pressure to 5.0 MPa by injecting methane into the specimen and kept the effective confining pressure at 0.2 MPa during this process. After that, reduced the temperature to 287.15 K to generate the hydrate. (3) Water saturation: water was injected from the bottom of the specimen to displace the free gas, changing the specimen to water-saturated state. (4) Consolidation: the pore

and confining pressure were increased to 10.0 and 13.0 MPa, respectively, to perform the consolidation test. (5) Shear test: the drained shear test with a constant axial loading rate was performed after consolidation. (6) Decomposition gas collection: decomposed the hydrate and collected the decomposition gas by increasing the temperature, and the hydrate saturation was calculated based on the volume of the decomposition gas. The specific experimental conditions are shown in Table 1. The hydrate saturation is around 0%, 15% and 40%, respectively, and the cell pressure is 13.0 MPa, with an effective confining pressure of 3.0 MPa. The temperature is 283.15 K, and three different strain rates are applied in this study (0.05, 0.5, and 1%/min).

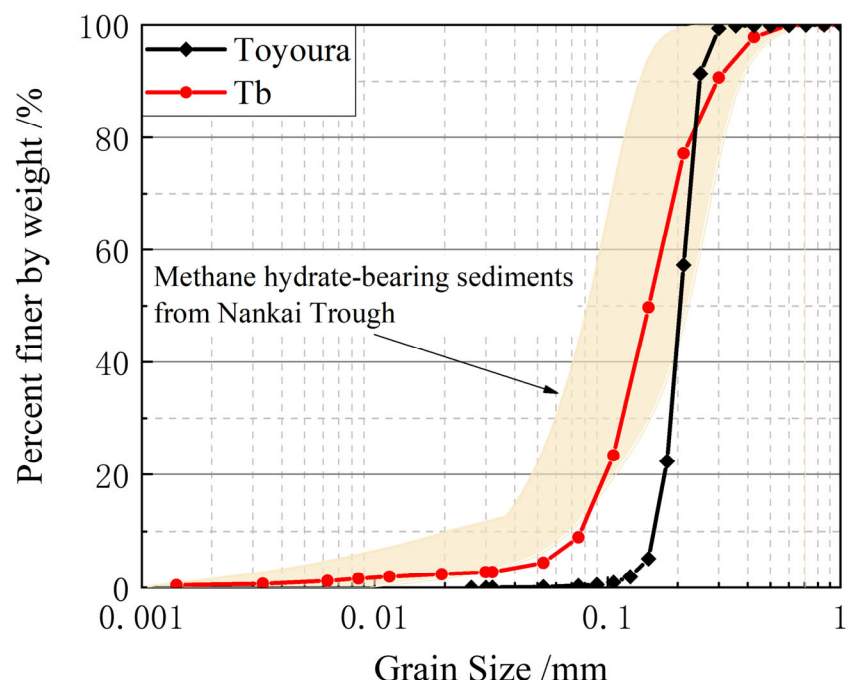


Figure 2. Grain size distribution of Toyoura and Tb.

Table 1. Experimental parameters and conditions.

Test	Host Sand	Hydrate Saturation (%)	Cell Pressure (MPa)	Pore Pressure (MPa)	Temperature (K)	Strain Rate (%/min)
1	Toyoura	0	13.0	10.0	283.15	0.05
2	Toyoura	0	13.0	10.0	283.15	0.5
3	Toyoura	0	13.0	10.0	283.15	1
4	Toyoura	11.6	13.0	10.0	283.15	0.05
5	Toyoura	16.3	13.0	10.0	283.15	0.5
6	Toyoura	12.4	13.0	10.0	283.15	1
7	Toyoura	43.6	13.0	10.0	283.15	0.05
8	Toyoura	42.5	13.0	10.0	283.15	0.5
9	Toyoura	43.7	13.0	10.0	283.15	1
10	Tb	0	13.0	10.0	283.15	0.05
11	Tb	0	13.0	10.0	283.15	0.5
12	Tb	0	13.0	10.0	283.15	1
13	Tb	43.6	13.0	10.0	283.15	0.05
14	Tb	40.0	13.0	10.0	283.15	0.5
15	Tb	44.3	13.0	10.0	283.15	1

3. Results

3.1. Stress–Strain Behavior

The left portion of Figure 3 presents the stress–strain relationship of the host Toyoura sand and the hydrate-bearing sediments with a low hydrate saturation under different strain rates. Under the same strain rate, the existence of a small amount of hydrate can slightly increase the peak strength, initial stiffness, and residual strength of the hydrate-bearing sediments. With respect to volumetric strain (where positive values indicate compression), all samples exhibit similar volumetric compressive behaviors, except for the host Toyoura sand, which displays a more pronounced volumetric compressive behavior at a strain rate of 0.05%/min. The strain rate shows slight effect on the stress–strain curves of the host Toyoura sand and the hydrate-bearing sediments with a low hydrate saturation. The right portion of Figure 3 shows the stress–strain relationship of the host Toyoura sand and the hydrate-bearing sediments with a high hydrate saturation. In this case, the peak strength, initial stiffness, and residual strength of the hydrate-bearing sediments increase significantly due to the existence of hydrate, and the stress–strain behavior of hydrate-bearing sediments is also greatly affected by the strain rate. At a high strain rate (1%/min), the peak strength and initial stiffness of the hydrate-bearing sediment are significantly increased. With regard to volumetric strain, there is an increase in both hydrate saturation and strain rate facilitated volumetric expansion behavior in the hydrate-bearing sediments.

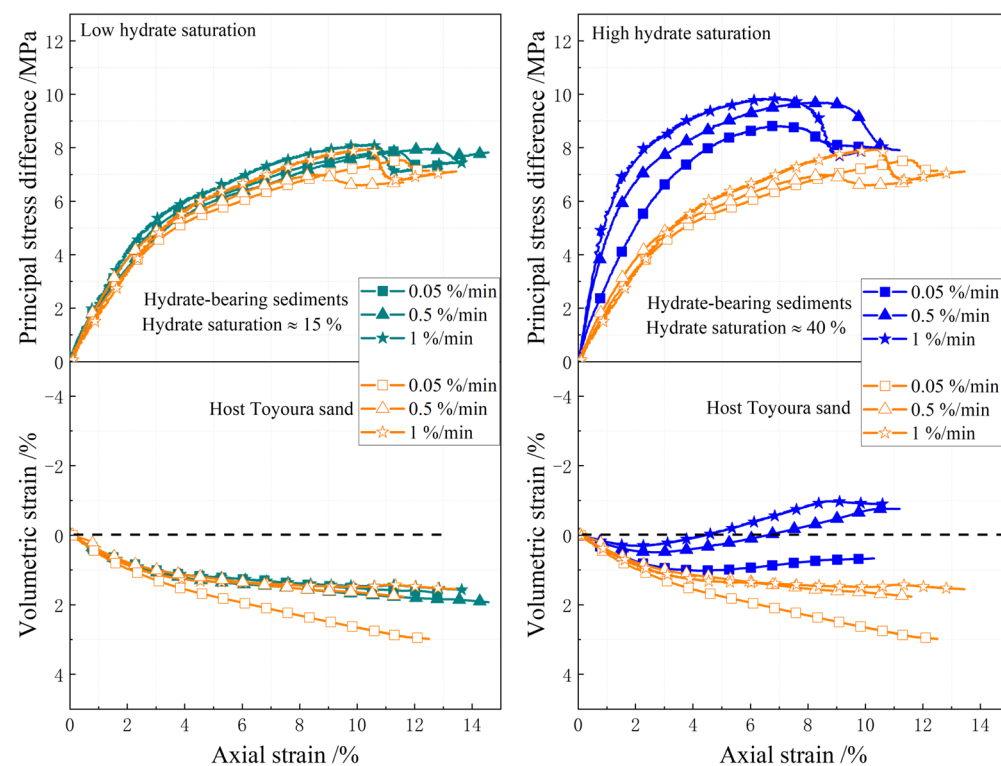


Figure 3. Stress–strain relationship of the hydrate-bearing sediments and host Toyoura sand under different strain rates.

Figure 4 shows the stress–strain relationship of the hydrate-bearing sediments (Toyoura and Tb) and the host sand (Toyoura and Tb). As can be seen in the left portion of Figure 4, the presence of fine particles reduced the initial stiffness and facilitated the volume compression behavior of host Tb sand. Volumetric compression was found to be most significant at a strain rate of 0.05%/min, consistent with the results obtained for the host Toyoura sand. The right portion of Figure 4 compared the stress–strain behavior of hydrate-bearing sediments (Toyoura and Tb) with a high hydrate saturation. The stress–strain behavior of hydrate-bearing sediments with fine particles also has strong strain rate

dependence; however, under the same strain rate conditions, the presence of fine particles reduces the initial stiffness and volume expansion effect of the hydrate-bearing sediments.

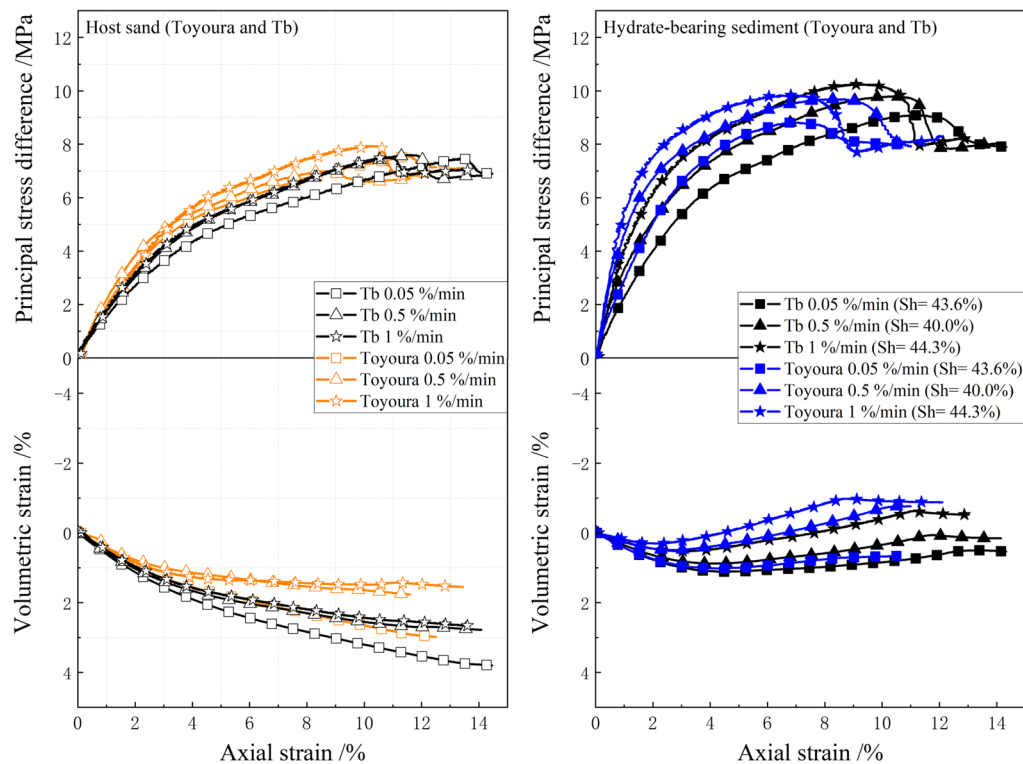


Figure 4. Stress–strain relationship of the hydrate-bearing sediments (Toyoura and Tb) and the host sand (Toyoura and Tb).

3.2. Effects of Hydrate Saturation

The influence of hydrate saturation on the strain rate dependence of hydrate-bearing sediments is further discussed in this part. Figure 5 presents the variation in the peak strength, the strain rate-dependent parameter, secant Young's modulus (E_{50}), and the residual strength of hydrate-bearing sediments and host Toyoura sand at different strain rates. The strain rate-dependent parameter, m , is commonly used to quantify the sensitivity of material strength to strain rate. It represents the slope of the relationship between material strength and strain rate in a log–log coordinate system [32]. In Figure 5a, unlike host Toyoura sands, the peak strength of hydrate-bearing sediments significantly increases with the increase in strain rate, and this phenomenon becomes more pronounced with the increase in hydrate saturation. For instance, when the hydrate saturation is approximately 40%, the peak strength of the hydrate-bearing sediment increases by 10% with a change in strain rate from 0.05%/minute to 0.5%/minute, while it increases by only 4% when the hydrate saturation is approximately 15%. The sensitivity of peak strength of hydrate-bearing sediments to strain rate increasing with the increase in hydrate saturation can also be observed in Figure 5b. Additionally, E_{50} significantly increases with the increase in strain rate when the hydrate saturation is high (40%). The residual strength only increases with the increase in hydrate saturation, regardless of the strain rate.

At a low hydrate saturation, hydrate exists on the pore and surface of sediment particles with little bridging of the sediments. With the increase in hydrate saturation, hydrate may also cover sediment particles to form clusters and play a load-bearing role [30]. The presence of hydrates can hinder the relative motion of sediment particles during shearing. Under high strain rate conditions, the sediment particles trapped within the hydrate structure may not have enough time to flip or move to adjacent locations. As a result, the stiffness and strength of the hydrate-bearing sediment are enhanced. Especially

for sediments with high hydrate saturation, the cementation effect of hydrate is stronger, and the hydrate that plays a load-bearing role itself may also have higher strength at a high strain rate [35]. The shear resistance of sediments is mainly affected by the hydrate that fills in the meniscus and pores, so the strain rate dependence of the hydrate itself may be the main reason for the strain rate dependence property of hydrate-bearing sediments [36]. In addition, it is also found that ice, which has similar physical properties to hydrates, has a certain strain rate dependence [37].

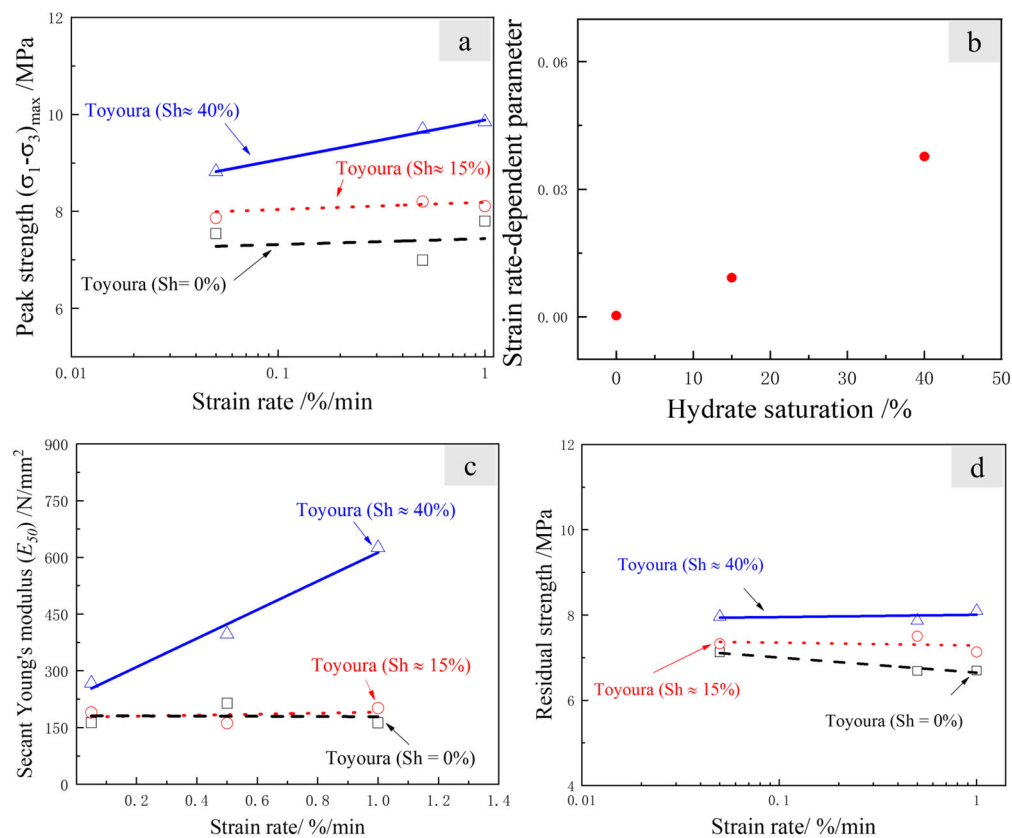


Figure 5. Variation in (a) the peak strength, (b) the strain rate-dependent parameter, (c) the secant Young's modulus (E_{50}), and (d) the residual strength of hydrate-bearing sediments and host Toyoura sand at different strain rates.

Figure 6 shows the schematic diagram of the shear band angle measurement method and the shear band angle results of hydrate-bearing sediments and host Toyoura sand at different strain rates. For host Toyoura sand, the angle of the shear band increases significantly when the strain rate changes from 0.05%/min to 0.5%/min. For the hydrate-bearing sediments with a low hydrate saturation, the strain rate has no effect on the shear band angle, and when the strain rate is greater than 0.05%/min, the shear band angle of the hydrate-bearing sediments is smaller than that of the host Toyoura sand. In the hydrate-bearing sediments with a high hydrate saturation, the angle of the shear band increases significantly, but the strain rate also has no significant effect on it. This implies that when the sediment contains hydrate, the angle of the shear band is independent of the strain rate; however, the hydrate saturation and the shear band angle of the sediments cannot be simply described by a positive correlation because they may have opposite laws under different strain rates.

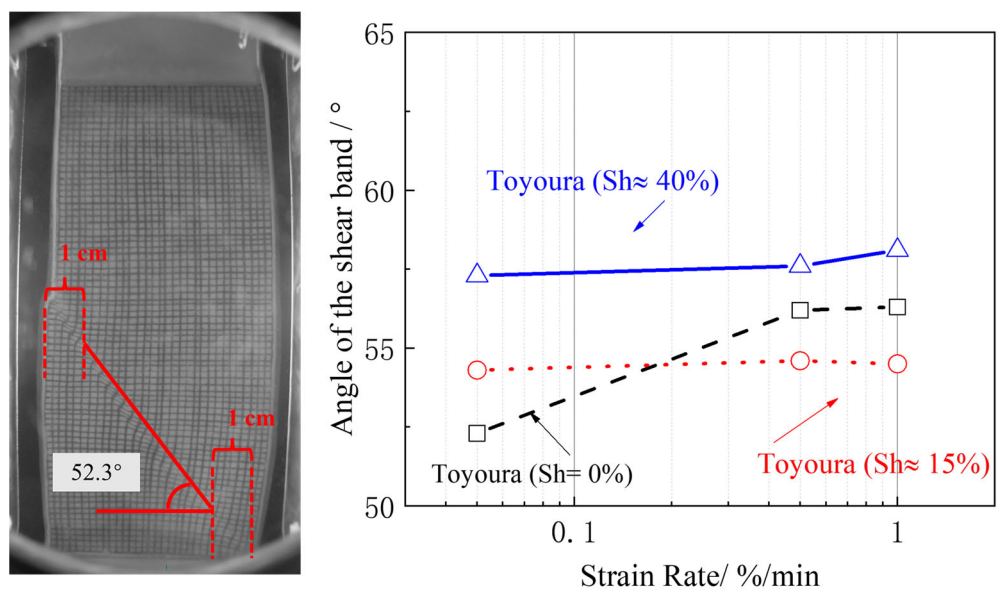


Figure 6. The schematic diagram of shear band angle measurement method (**left**) and the shear band angle results of hydrate-bearing sediments and host Toyoura sand at different strain rates (**right**).

The volumetric strain behavior of hydrate-bearing sediments with low hydrate saturation is similar to that of host Toyoura sand (see Figure 3). Figure 7 only shows the contours of the volumetric strain of hydrate-bearing sediments with a high hydrate saturation and host Toyoura sand at the critical state stage [38]. Compared with the host Toyoura sand, the hydrate-bearing sediments with a high hydrate saturation have more significant local volume expansion with the increase in strain rate. This is consistent with the result in Figure 5 that the volume expansion of hydrate-bearing sediments with high hydrate saturation is more pronounced with increasing strain rate. Yoneda et al. (2016) found that the movement of sediment particles can compress as well as dilate the sample in the shear band area, and the particle structure changes in the shear band position were much more significant than those in the non-shear band position [39]. The presence of hydrates makes the sediment more compact, and the relatively fast movement of sediment particles may tend to dilate the sample under high strain rate conditions.

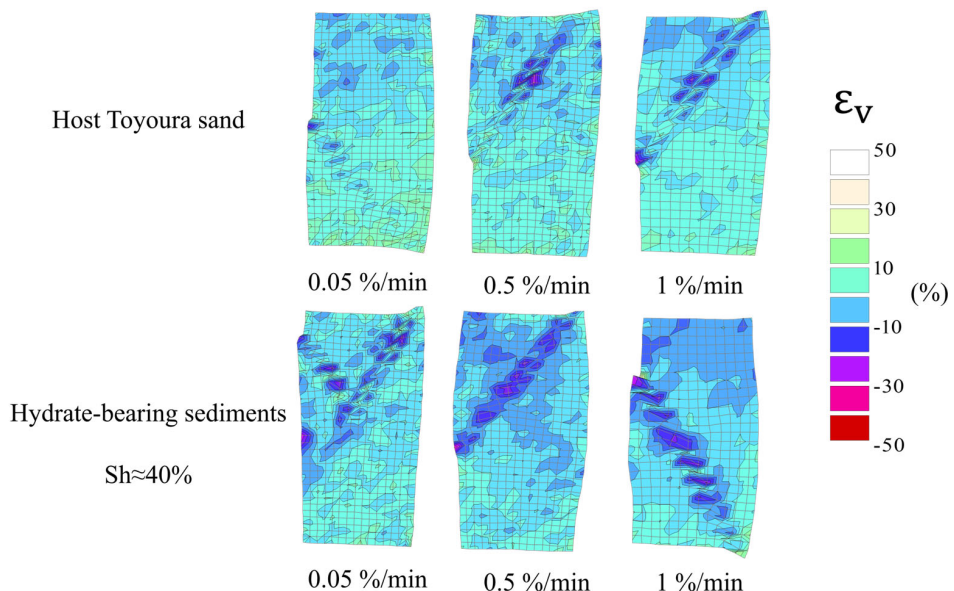


Figure 7. The contours of volumetric strain of hydrate-bearing sediments with a high hydrate saturation and host Toyoura sand at the critical state stage (positive values represent compression).

3.3. Effects of Fine Particles

The influence of fine particles on the strain rate dependence of hydrate-bearing sediments is further discussed in this part. The variation in the peak strength, strain rate-dependent parameter, secant Young's modulus (E_{50}), and the residual strength of hydrate-bearing sediments (Toyoura and Tb) and host sand (Toyoura and Tb) at different strain rate are shown in Figure 8. In Figure 8a, the presence of fine particles slightly increases the peak strength of hydrate-bearing sediments, and this is consistent with the previously reported findings by Kajiyama et al. (2017) [12]. Figure 8b compares the results of triaxial shear tests and plane strain tests on the strain rate sensitivity of peak strength for hydrate-bearing sediments. Although the strain rate sensitivity of peak strength for hydrate-bearing sediments increases under both stress conditions, the magnitude of the increase is smaller under plane strain conditions. In Figure 8c, compared to the hydrate-bearing sediments (Toyoura), the hydrate-bearing sediments (Tb) exhibited a higher E_{50} and were less sensitive to changes in strain rate. Additionally, the presence or absence of fine particles had no effect on the residual strength of host sand and hydrate-bearing sediments in this study (Figure 8d).

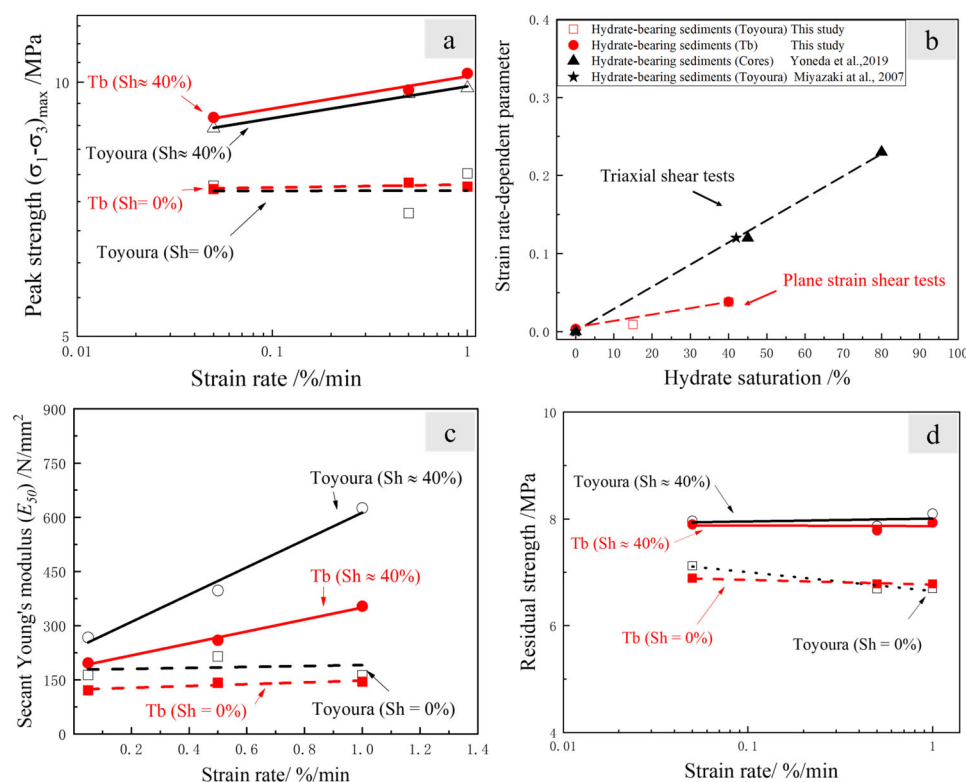


Figure 8. Variation in (a) the peak strength, (b) the strain rate-dependent parameter, (c) the secant Young's modulus (E_{50}), and (d) the residual strength of hydrate-bearing sediments (Toyoura and Tb) and host sand (Toyoura and Tb) at different strain rates.

Sediments containing fine particles are more prone to the formation of bonded clusters, which subsequently enhances the sediment's shear strength. Lei et al. (2017) also reported that even a small number of fine particles can significantly affect the formation of hydrates in sediments, thereby affecting their mechanical properties [16]. Based on this, a plausible explanation is that under low strain rate conditions, the bonded clusters have enough time to move along with the sediment particles as a cohesive unit, whereas under high strain rate conditions, the particles' motion must overcome the resistance of the bonded clusters, leading to a greater shear strength.

Figure 9 shows the shear band angle results of hydrate-bearing sediments (Toyoura and Tb) and host sand (Toyoura and Tb) at different strain rates. For host Tb sand, the angle of its shear band increases slightly with increasing strain rate, which is consistent with the

results for host Toyoura sand; however, the shear band angle of hydrate-bearing sediments first increases and then decreases with the increase in strain rate. This finding suggests that alterations in hydrate saturation and fines content have the potential to impact the correlation between strain rate and shear band angle. Previous studies have also shown that changes in the swelling angle and the complex cementation mechanism between hydrate and sediment particles can affect the changes in the shear band angle.

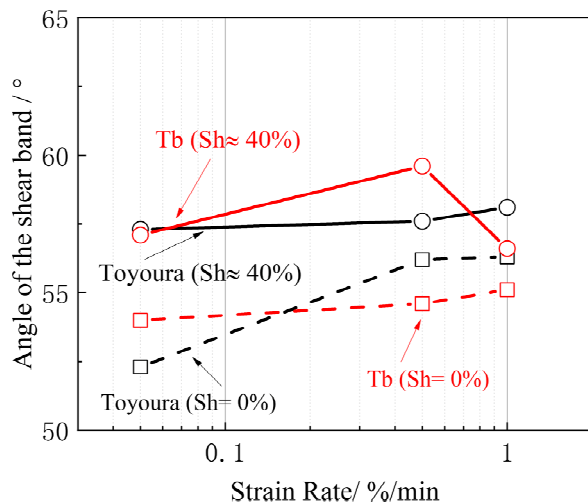


Figure 9. The shear band angle results of hydrate-bearing sediments (Toyoura and Tb) and host sand (Toyoura and Tb) at different strain rates.

The contours of the volumetric strain of hydrate-bearing sediments and host Tb sand at the critical state stage are shown in Figure 10. Compared to the result of host Toyoura and hydrate-bearing sediments (Toyoura) in Figure 7, under a higher strain rate, the local volumetric expansion area of the host sand (Tb) and hydrate-bearing sediments (Tb) is slightly reduced and increased, respectively. This means that the strain rate has little effect on the local volumetric strain of the samples (Tb), regardless of hydrate presence. Additionally, the local volumetric strain expansion of the hydrate-bearing sediments (Toyoura) is more significant than that of the hydrate-bearing sediments (Tb) under all strain rate conditions.

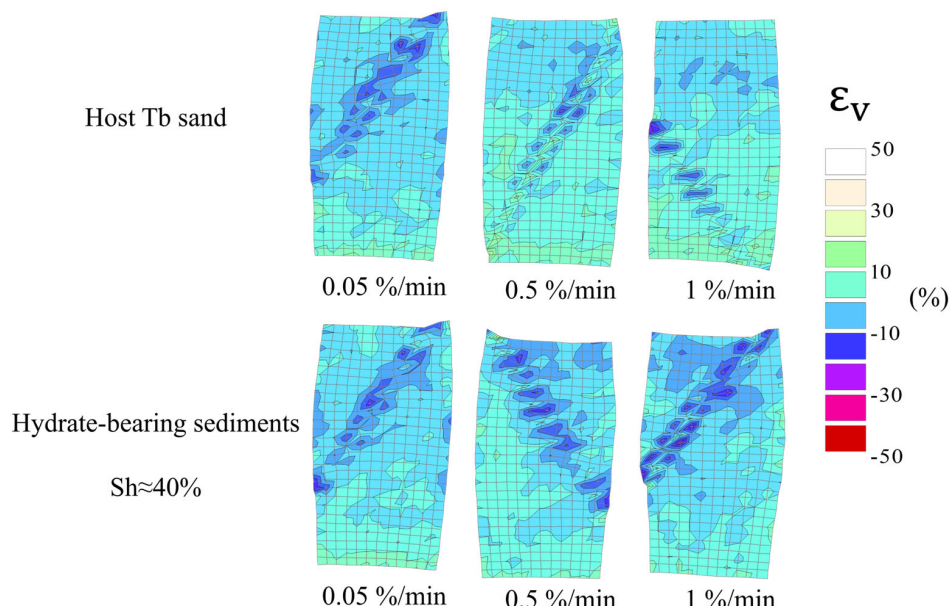


Figure 10. The contours of volumetric strain of hydrate-bearing sediments and host Tb sand at the critical state stage.

4. Discussion

Based on the previous experimental results and earlier research findings, this section analyzes the strain rate dependence mechanism of the mechanical properties of hydrate-bearing sediments under plane strain conditions.

Firstly, the mechanical properties of hydrate itself exhibit high strain rate dependence. The strain rate dependence parameter, m , of pure hydrate samples can reach 0.46 [35], which means that their strain rate sensitivity far exceeds that of hydrated sediment samples. Hydrate itself may dominate the strain rate dependence of the hydrated sediment samples ($m = 0.12$) [32]. Previous experimental results have shown that the saturation of hydrates is positively correlated with the strain rate sensitivity of hydrated sediment samples, which confirms this point (Figure 5b).

As the saturation of hydrates increases, some hydrates may replace the positions of sediment particles and support the sediment structures [40,41]. This portion of hydrates can significantly increase the strain rate dependence of the entire sample due to its own high strain rate sensitivity. In addition, during the shearing process, as particles move, some of the hydrates existing between particle pores can also be filled between particles. This not only prevents particles from further movement, but it also increases the strain rate dependence of the hydrate-bearing sediments. Under high strain rate conditions, the movement of sediment particles becomes more difficult due to the higher binding force of hydrates, which easily leads to stress concentration. During the shear process, microcracks are further formed, resulting in an increase in the volume expansion effect of the sample. Regardless, the hydrates that lose their cementing effect during the shear process stagnate on the surface of sediment particles, which also increases the local volume expansion effect of the sample [42].

Filling fine particles among sediment reduces the pore size between sediment particles and thereby may affect the morphology of hydrates [43–45]. Previous studies have found that even a small number of fines in sediments can significantly affect the mechanical properties and transport response of hydrate-bearing sediments. Hydrates tend to form in the pores of coarse sediments without fines without changing the sediment structure. When the pores between sediment particles are occupied by fines, hydrates tend to displace sediment particles due to the higher capillary pressure, leading to the formation of segregated hydrates [16]. The hydrates in the pores contribute little to the mechanical properties of sediments, and only when the sediment particles are compressed and displaced, this portion of hydrates significantly affects the strength of the sediments. This also explains why the presence of fines only affects the peak strength, not the residual strength, of hydrate-bearing sediments. Furthermore, in this study, it was found that the presence of fines does not affect the strain rate sensitivity of the peak strength of hydrate-bearing sediments. This also implies that the strain rate dependence of hydrate-bearing sediments is more influenced by the content of hydrates in sediments than by their morphologies. Microscopic experiments under similar conditions need to be conducted to directly observe the effects of hydrate and fine particle content on the internal structure changes of hydrate-bearing sediments under different strain rate conditions and further clarify the mechanism of the strain rate dependence of the mechanical properties of hydrate-bearing sediments.

5. Conclusions

In this study, a series of plane strain shear tests at different strain rates were performed, and the influence of hydrate and fine particle contents on the strain rate dependence of hydrate-bearing sediments was studied. Based on the experimental results, the following conclusions can be reached:

(1) With an increase in hydrate saturation, the stress-strain behaviors of hydrate-bearing sediments are significantly affected by the strain rate, particularly in sediments that lack fine particles. Under plane strain conditions, the strain rate sensitivity of the mechanical properties of hydrate-bearing sediments is lower than that under triaxial conditions.

(2) The peak strength and E_{50} of hydrate-bearing sediments with high hydrate saturation increase with an increase in strain rate, regardless of whether or not they contain fine particles; however, the presence of fine particles reduces the strain rate dependence of E_{50} for hydrate-bearing sediments. The residual strength of hydrate-bearing sediments is primarily controlled by the hydrate saturation and is independent of the strain rate.

(3) Hydrate-bearing sediments with high hydrate saturation have larger shear band angles, and the angle of the shear bands can also be influenced by the combined effects of fine particles and strain rate.

(4) An increase in hydrate saturation or the presence of fine particles leads to a reduction in the degree of local volume expansion of hydrate-bearing sediments.

Author Contributions: Conceptualization, Q.W. and J.G.; methodology, Q.W., Y.Z. and J.G.; validation, N.Y. and Y.N.; formal analysis, S.K. and M.H.; investigation, N.Y. and S.K.; data curation, N.Y., Y.N. and S.K.; writing—original draft preparation, Q.W.; writing—review and editing, Q.W. and J.G.; supervision, J.G.; project administration, M.H.; funding acquisition, J.G. and M.H. All authors have read and agreed to the published version of the manuscript.

Funding: This work was jointly supported by the Natural Science Foundation of Guangdong Province, China (2021A1515011515), China Scholarship Council (202104910252), Japan Ministry of Education, Culture, Sports, Science and Technology (Grant-in-Aid for Scientific Research (C) No. 20K04683), the Electric Technology Research Foundation of Chugoku, the Open Research Fund of National Center for International Research on Deep Earth Drilling and Resource Development, Ministry of Science and Technology (DEDRD-2022-01).

Institutional Review Board Statement: Not applicable.

Informed Consent Statement: Not applicable.

Data Availability Statement: The data that support the findings of this study are available within the article.

Conflicts of Interest: The authors declare no conflict of interest.

References

1. Moridis, G.J.; Collett, T.S.; Pooladi-Darvish, M.; Hancock, S.; Santamarina, C.; Boswell, R.; Kneafsey, T.; Rutqvist, J.; Kowalsky, M.B.B.; Reagan, M.T.T.; et al. Challenges, uncertainties, and issues facing gas production from gas-hydrate deposits. *SPE Reserv. Eval. Eng.* **2011**, *14*, 76–112. [[CrossRef](#)]
2. Zhang, X.H.; Luo, D.S.; Lu, X.B.; Liu, L.L.; Liu, C.L. Mechanical properties of gas hydrate-bearing sediments during hydrate dissociation. *Acta Mech. Sin.* **2018**, *34*, 266–274. [[CrossRef](#)]
3. Holder, G.D.; Angert, P.F. Simulation of gas production from a reservoir containing both gas hydrates and free natural gas. In Proceedings of the SPE Annual Technical Conference and Exhibition SPE-11105-MS, New Orleans, LA, USA, 26–29 September 1982.
4. Urdahl, O.; Lund, A.; Mørk, P.; Nilsen, T. Inhibition of gas hydrate formation by means of chemical additives—I. Development of an experimental set-up for characterization of gas hydrate inhibitor efficiency with respect to flow properties and deposition. *Chem. Eng. Sci.* **1995**, *50*, 863–870. [[CrossRef](#)]
5. Rossi, F.; Gambelli, A.M.; Sharma, D.K.; Castellani, B.; Nicolini, A.; Castaldi, M.J. Experiments on methane hydrates formation in seabed deposits and gas recovery adopting carbon dioxide replacement strategies. *Appl. Therm. Eng.* **2019**, *148*, 371–381. [[CrossRef](#)]
6. Ye, J.; Qin, X.; Xie, W.; Lu, H.; Ma, B.; Qiu, H.; Liang, J.-Q.; Lu, J.-A.; Kuang, Z.-G.; Lu, C.; et al. The second natural gas hydrate production test in the South China Sea. *China Geol.* **2020**, *3*, 197–209. [[CrossRef](#)]
7. Fujii, T.; Suzuki, K.; Takayama, T.; Tamaki, M.; Komatsu, Y.; Konno, Y.; Yoneda, J.; Yamamoto, K.; Nagao, J. Geological setting and characterization of a methane hydrate reservoir distributed at the first offshore production test site on the Daini-Atsumi Knoll in the eastern Nankai Trough, Japan. *Mar. Pet. Geol.* **2015**, *66*, 310–322. [[CrossRef](#)]
8. Li, Y.; Wu, N.; Gao, D.; Chen, Q.; Liu, C.; Yang, D.; Jin, Y.; Ning, F.; Tan, M.; Hu, G. Optimization and analysis of gravel packing parameters in horizontal wells for natural gas hydrate production. *Energy* **2021**, *219*, 119585. [[CrossRef](#)]
9. Yan, C.; Ren, X.; Cheng, Y.; Song, B.; Li, Y.; Tian, W. Geomechanical issues in the exploitation of natural gas hydrate. *Gondwana Res.* **2020**, *81*, 403–422. [[CrossRef](#)]
10. Fetisov, V.; Gonopolsky, A.M.; Davardoost, H.; Ghanbari, A.R.; Mohammadi, A.H. Regulation and impact of VOC and CO₂ emissions on low-carbon energy systems resilient to climate change: A case study on an environmental issue in the oil and gas industry. *Energy Sci. Eng.* **2023**, *11*, 1516–1535. [[CrossRef](#)]

11. Hyodo, M.; Li, Y.; Yoneda, J.; Nakata, Y.; Yoshimoto, N.; Nishimura, A.; Song, Y. Mechanical behavior of gas-saturated methane hydrate-bearing sediments. *J. Geophys. Res. Solid Earth* **2013**, *118*, 5185–5194. [[CrossRef](#)]
12. Kajiyama, S.; Hyodo, M.; Nakata, Y.; Yoshimoto, N.; Wu, Y.; Kato, A. Shear behaviour of methane hydrate bearing sand with various particle characteristics and fines. *Soils Found.* **2017**, *57*, 176–193. [[CrossRef](#)]
13. Winters, W.J.; Waite, W.F.; Mason, D.H.; Gilbert, L.Y.; Pecher, I.A. Methane gas hydrate effect on sediment acoustic and strength properties. *J. Pet. Sci. Eng.* **2007**, *56*, 127–135. [[CrossRef](#)]
14. Liu, Z.; Dai, S.; Ning, F.; Peng, L.; Wei, H.; Wei, C. Strength estimation for hydrate-bearing sediments from direct shear tests of hydrate-bearing sand and silt. *Geophys. Res. Lett.* **2018**, *45*, 715–723. [[CrossRef](#)]
15. Lv, J.; Zhao, J.; Jiang, L.; Liu, Y.; Mu, H. A review of micro computed tomography studies on the gas hydrate pore habits and seepage properties in hydrate bearing sediments. *J. Nat. Gas Sci. Eng.* **2020**, *83*, 103555. [[CrossRef](#)]
16. Lei, L.; Santamarina, J.C. Physical properties of fine-grained sediments with segregated hydrate lenses. *Mar. Pet. Geol.* **2019**, *109*, 899–911. [[CrossRef](#)]
17. Li, Y.; Song, Y.; Liu, W.; Yu, F.; Wang, R. A new strength criterion and constitutive model of gas hydrate-bearing sediments under high confining pressures. *J. Pet. Sci. Eng.* **2013**, *109*, 45–50. [[CrossRef](#)]
18. Song, Y.; Zhu, Y.; Liu, W.; Li, Y.; Lu, Y.; Shen, Z. The effects of methane hydrate dissociation at different temperatures on the stability of porous sediments. *J. Pet. Sci. Eng.* **2016**, *147*, 77–86. [[CrossRef](#)]
19. Yan, C.; Cheng, Y.; Li, M.; Han, Z.; Zhang, H.; Li, Q.F.; Teng, F.; Ding, J. Mechanical experiments and constitutive model of natural gas hydrate reservoirs. *Int J Hydrogen Energy* **2017**, *42*, 19810–19818. [[CrossRef](#)]
20. Dou, X.; Liu, Z.; Ning, F.; Li, Y.; Li, X.; Zhao, Y.; Hu, W.; Gao, D. 3D DEM modeling on mechanical weakening of gas hydrate-bearing sandy sediments during hydrate dissociation. *Comput. Geotech.* **2023**, *154*, 105116. [[CrossRef](#)]
21. Wu, Q.; Dou, X.; Zhao, Y.; Liu, Z.; Li, Y.; Yoshimoto, N.; Ning, F. Discrete element simulation of the hydrate-bearing sediments mechanical behaviors under typical hydrate dissociation patterns. *Gas Sci. Eng.* **2023**, *115*, 205020. [[CrossRef](#)]
22. Zhou, J.; Yang, Z.; Wei, C.; Chen, P.; Yan, R. Mechanical behavior of hydrate-bearing sands with fine particles under isotropic and triaxial compression. *J. Nat. Gas Sci. Eng.* **2021**, *92*, 103991. [[CrossRef](#)]
23. Hyodo, M.; Wu, Y.; Nakashima, K.; Kajiyama, S.; Nakata, Y. Influence of fines content on the mechanical behavior of methane hydrate-bearing sediments. *J. Geophys. Res. Solid Earth* **2017**, *122*, 7511–7524. [[CrossRef](#)]
24. Song, Y.; Zhu, Y.; Liu, W.; Zhao, J.; Li, Y.; Chen, Y.; Shen, Z.; Lu, Y.; Ji, C. Experimental research on the mechanical properties of methane hydrate-bearing sediments during hydrate dissociation. *Mar. Pet. Geol.* **2014**, *51*, 70–78. [[CrossRef](#)]
25. Klar, A.; Soga, K.; Ng, M.Y.A. Coupled deformation–flow analysis for methane hydrate extraction. *Geotechnique* **2010**, *60*, 765–776. [[CrossRef](#)]
26. Pinkert, S. Rowe's stress-dilatancy theory for hydrate-bearing sand. *Int. J. Geomech.* **2017**, *17*, 06016008. [[CrossRef](#)]
27. Yu, F.; Song, Y.; Liu, W.; Li, Y.; Lam, W. Analyses of stress strain behavior and constitutive model of artificial methane hydrate. *J. Pet. Sci. Eng.* **2011**, *77*, 183–188. [[CrossRef](#)]
28. Uchida, S.; Soga, K.; Yamamoto, K. Critical state soil constitutive model for methane hydrate soil. *J. Geophys. Res. Solid Earth* **2012**, *117*, B03209. [[CrossRef](#)]
29. Sánchez, M.; Gai, X.; Santamarina, J.C. A constitutive mechanical model for gas hydrate bearing sediments incorporating inelastic mechanisms. *Comput. Geotech.* **2017**, *84*, 28–46. [[CrossRef](#)]
30. Lijith, K.P.; Malagar, B.R.C.; Singh, D.N. A comprehensive review on the geomechanical properties of gas hydrate bearing sediments. *Mar. Pet. Geol.* **2019**, *104*, 270–285. [[CrossRef](#)]
31. Iwai, H.; Konishi, Y.; Saimyou, K.; Kimoto, S.; Oka, F. Rate effect on the stress-strain relations of synthetic carbon dioxide hydrate-bearing sand and dissociation tests by thermal stimulation. *Soils Found.* **2018**, *58*, 1113–1132. [[CrossRef](#)]
32. Miyazaki, K.; Tenma, N.; Yamaguchi, T. Relationship between creep property and loading-rate dependence of strength of artificial methane-hydrate-bearing toyoura sand under triaxial compression. *Energies* **2017**, *10*, 1466. [[CrossRef](#)]
33. Gao, Y.; Yang, M.; Zheng, J.; Chen, C. Production characteristics of two class water-excess methane hydrate deposits during depressurization. *Fuel* **2018**, *232*, 99–107. [[CrossRef](#)]
34. Yoneda, J.; Hyodo, M.; Yoshimoto, N.; Nakata, Y.; Kato, A. Development of high-pressure low-temperature plane strain testing apparatus for methane hydrate-bearing sand. *Soils Found.* **2013**, *53*, 774–783. [[CrossRef](#)]
35. Durham, W.B.; Kirby, S.H.; Stern, L.A.; Zhang, W. The strength and rheology of methane clathrate hydrate. *J. Geophys. Res. Solid Earth* **2003**, *108*, 2182. [[CrossRef](#)]
36. Yoneda, J.; Oshima, M.; Kida, M.; Kato, M.; Konno, Y.; Jin, Y.; Jang, J.; Waite, W.F.; Kumar, P.; Tenma, N. Pressure core based onshore laboratory analysis on mechanical properties of hydrate-bearing sediments recovered during India's National Gas Hydrate Program Expedition (NGHP) 02. *Mar. Pet. Geol.* **2019**, *108*, 482–501. [[CrossRef](#)]
37. Jones, S.J. High strain-rate compression tests on ice. *J. Phys. Chem. B* **1997**, *101*, 6099–6101. [[CrossRef](#)]
38. Liu, H.; Song, E.; Ling, H.I. Constitutive modeling of soil-structure interface through the concept of critical state soil mechanics. *Mech. Res. Commun.* **2006**, *33*, 515–531. [[CrossRef](#)]
39. Yoneda, J.; Jin, Y.; Katagiri, J.; Tenma, N. Strengthening mechanism of cemented hydrate-bearing sand at microscales. *Geophys. Res. Lett.* **2016**, *43*, 7442–7450. [[CrossRef](#)]
40. Yun, T.S.; Santamarina, J.C.; Ruppel, C. Mechanical properties of sand, silt, and clay containing tetrahydrofuran hydrate. *J. Geophys. Res. Solid Earth* **2007**, *112*, B04106. [[CrossRef](#)]

41. Dai, S.; Santamarina, J.C.; Waite, W.F.; Kneafsey, T.J. Hydrate morphology: Physical properties of sands with patchy hydrate saturation. *J. Geophys. Res. Solid Earth* **2012**, *117*, B11205. [[CrossRef](#)]
42. Wu, P.; Li, Y.; Liu, W.; Sun, X.; Kong, X.; Song, Y. Cementation failure behavior of consolidated gas hydrate-bearing sand. *J. Geophys. Res. Solid Earth* **2020**, *125*, e2019JB018623. [[CrossRef](#)]
43. Booth, J.S.; Winters, W.J.; Dillon, W.P.; Clennell, M.B.; Rowe, M.M. Major occurrences and reservoir concepts of marine clathrate hydrates: Implications of field evidence. *Geol. Soc. Spec. Publ.* **1998**, *137*, 113–127. [[CrossRef](#)]
44. Clennell, M.B.; Hovland, M.; Booth, J.S.; Henry, P.; Winters, W.J. Formation of natural gas hydrates in marine sediments: 1. Conceptual model of gas hydrate growth conditioned by host sediment properties. *J. Geophys. Res. Solid Earth* **1999**, *104*, 22985–23003.
45. Terzariol, M.; Park, J.; Castro, G.M.; Santamarina, J.S. Methane hydrate-bearing sediments: Pore habit and implications. *Mar. Pet. Geol.* **2020**, *116*, 104302. [[CrossRef](#)]

Disclaimer/Publisher's Note: The statements, opinions and data contained in all publications are solely those of the individual author(s) and contributor(s) and not of MDPI and/or the editor(s). MDPI and/or the editor(s) disclaim responsibility for any injury to people or property resulting from any ideas, methods, instructions or products referred to in the content.